Mineralogical Magazine, April 2018, Vol. 82(2), pp. 401–411

Greenlizardite, $(NH_4)Na(UO_2)_2(SO_4)_2(OH)_2{\cdot}4H_2O$, a new mineral with phosphuranylite-type uranyl sulfate sheets from Red Canyon, San Juan County, Utah, USA

Anthony R. Kampf[1,*], Jakub Plášil[2], Barbara P. Nash[3] and Joe Marty[4]

[1] Mineral Sciences Department, Natural History Museum of Los Angeles County, 900 Exposition Boulevard, Los Angeles, CA 90007, USA
[2] Institute of Physics ASCR, v.v.i., Na Slovance 1999/2, 18221 Praha 8, Czech Republic
[3] Department of Geology and Geophysics, University of Utah, Salt Lake City, Utah 84112, USA
[4] 5199 East Silver Oak Road, Salt Lake City, UT 84108, USA

[*Received 1 June 2017; Accepted 19 June 2017; Associate Editor: Stuart Mills*]

ABSTRACT

The new mineral greenlizardite (IMA2017-001), $(NH_4)Na(UO_2)_2(SO_4)_2(OH)_2{\cdot}4H_2O$, was found in the Green Lizard mine, Red Canyon, San Juan County, Utah, USA, where it occurs as a secondary alteration phase. It is associated with ammoniozippeite, boussingaultite and dickite. It forms as light green-yellow blades up to ~0.3 mm long. The mineral is vitreous and transparent with a white streak. It fluoresces greenish blue in 405 nm light. Mohs hardness is ~2. Crystals are brittle with irregular fracture and two cleavages: perfect {001} and good $\{2\bar{1}0\}$. Greenlizardite is easily soluble in room-temperature H_2O. The calculated density is 3.469 g cm^{-3}. Optically, it is biaxial (+) with $\alpha = 1.559(1)$, $\beta = 1.582(1)$ and $\gamma = 1.608(1)$ (measured in white light). The measured 2V is 88(1)°; the calculated 2V is 87.8°. Dispersion is moderate, $r < v$. Pleochroism is X = very pale yellow green, Y = pale yellow green and Z = light yellow green; $X < Y < Z$. The optical orientation is $X \approx \mathbf{c}$, $Y \approx \mathbf{a}$ and $Z \approx \mathbf{b}^*$. The Raman spectrum exhibits bands attributable to both sulfate and uranyl groups. Electron probe microanalyses (with H_2O based on the crystal structure) yielded $(NH_4)_{0.98}Na_{1.00}U_{1.96}S_{2.04}O_{18.00}H_{10.02}$. Greenlizardite is triclinic, $P\bar{1}$, $a = 6.83617(17)$, $b = 9.5127(3)$, $c = 13.8979(10)$ Å, $\alpha = 98.636(7)$, $\beta = 93.713(7)$, $\gamma = 110.102(8)°$, $V = 832.49(8)$ Å^3 and $Z = 2$. The crystal structure ($R_1 = 2.39\%$ for 2542 $I > 2\sigma I$) contains edge-sharing dimers of UO_7 pentagonal bipyramids. The dimers link by sharing corners with SO_4 groups to form a $[(UO_2)_2(SO_4)_2(OH)_2]^{2-}$ sheet based on the phosphuranylite anion topology. Zig-zag edge-sharing chains of NaO_6 octahedra link adjacent $[(UO_2)_2(SO_4)_2(OH)_2]^{2-}$ sheets, forming thick slabs. NH_4 bonds to O atoms in adjacent slabs linking them together. H_2O groups occupy channels in the slabs and space between the slabs.

Keywords: greenlizardite, new mineral, uranyl sulfate, crystal structure, Raman spectroscopy, Green Lizard mine, Red Canyon, Utah, USA.

Introduction

Our interest in the secondary mineralization in the uranium mines of Red Canyon in White canyon district of south-eastern Utah (USA) began several years ago at the Blue Lizard mine. That mine has now proven to be a prolific source for new mineral species, having already yielded 16, with several others still under study. We have expanded our efforts to several nearby mines including the Green Lizard, Giveaway-Simplot and Markey mines. All share similar geology and mineralogy, and some new species are found at more than one mine. We have provided a brief synopsis of the history of uranium mining in the area in our descriptive paper on shumwayite, a new mineral found at both the Green Lizard and Giveaway-Simplot mines (Kampf *et al.*, 2017). Herein, we describe

*E-mail: akampf@nhm.org
https://doi.org/10.1180/minmag.2017.081.054

greenlizardite, the second new mineral from the Green Lizard mine.

Greenlizardite is named for the locality, the Green Lizard mine. The new mineral and its name were approved by the Commission on New Minerals, Nomenclature and Classification of the International Mineralogical Association (IMA2017-001). The description is based on one holotype and one cotype specimen, which are deposited in the collections of the Natural History Museum of Los Angeles County, 900 Exposition Boulevard, Los Angeles, CA 90007, USA, catalogue numbers 66558 and 66559, respectively.

Occurrence

Greenlizardite was discovered on specimens collected underground in the Green Lizard mine (37°34'37.10"N, 110°17'52.80"W) in the White Canyon mining district, San Juan County, Utah, USA. The Green Lizard mine is near the head of Low Canyon on the east side of Red Canyon, 2.1 km north of the Blue Lizard mine. The geology is similar to that of the Blue Lizard mine (Kampf *et al*., 2015*a*; Chenoweth, 1993). The Green Lizard mine is also a cotype locality for shumwayite (Kampf *et al*., 2017).

Mineralized channels are in the Shinarump member of the Chinle Formation. The Shinarump member consists of medium- to coarse-grained sandstone, conglomeratic sandstone beds and thick siltstone lenses. Ore minerals were deposited as replacements of wood and other organic material and as disseminations in the enclosing sandstone. Since the mine closed, oxidation of primary ores in the humid underground environment has produced a variety of secondary minerals, mainly sulfates, as efflorescent crusts on the surfaces of mine walls.

Greenlizardite is a rare mineral, found in association with ammoniozippeite, boussingaultite, dickite and a potentially new Mg uranyl sulfate mineral, currently under study. Other secondary minerals found in the Green Lizard mine assemblage include beshtauite, calcite, gypsum, fermiite, johannite, natrozippeite, oppenheimerite, plášilite, rozenite, shumwayite, sulfur and wetherillite.

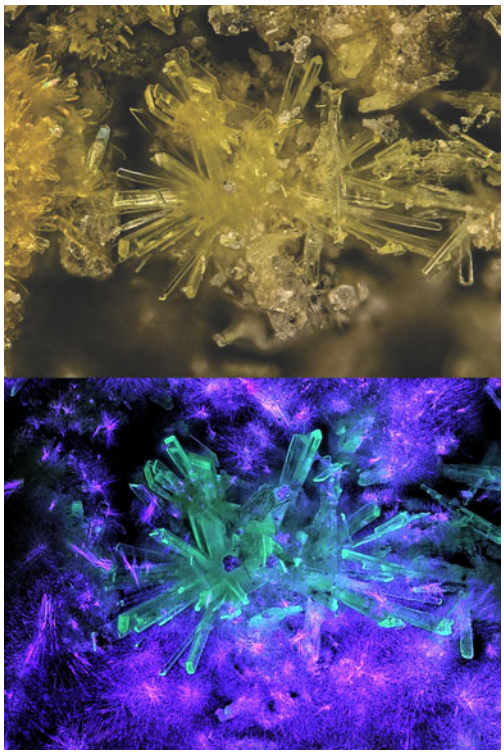

FIG. 1. Greenlizardite with ammoniozippeite (left) in incandescent light (top) and 405 nm ultraviolet light (bottom). The field of view is 0.84 mm across.

Physical and optical properties

Greenlizardite occurs as light green-yellow blades, up to ~0.3 mm long, forming irregular sprays (Fig. 1). Blades are flattened on {001}, elongated on [100] and exhibit the forms $\{\bar{1}00\}$, {010}, $\{0\bar{1}0\}$, {001}, $\{00\bar{1}\}$, $\{\bar{1}10\}$, $\{\bar{1}\bar{1}0\}$, $\{\bar{1}20\}$ and $\{2\bar{1}0\}$

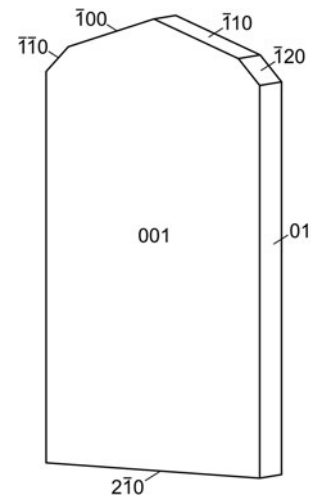

FIG. 2. Crystal drawing of greenlizardite, clinographic projection in nonstandard orientation.

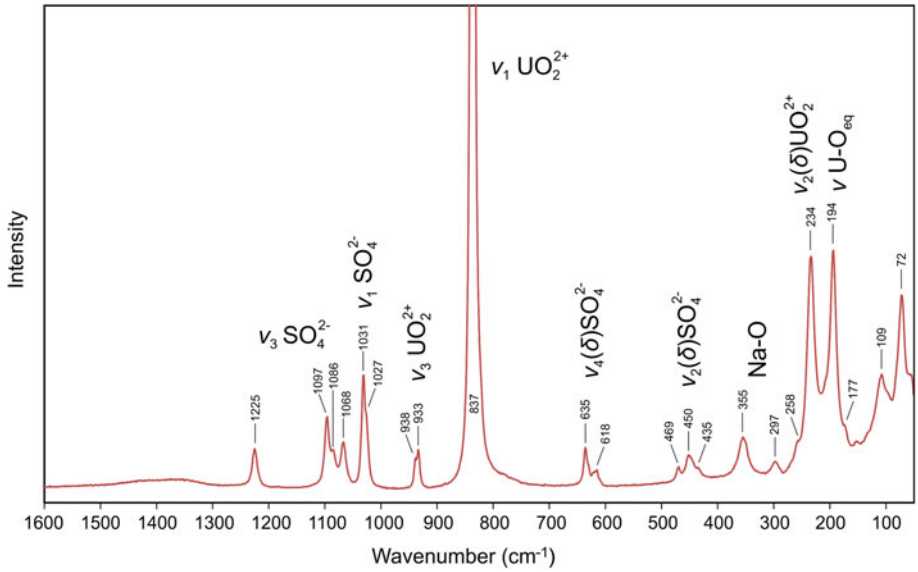

FIG. 3. Raman spectrum of greenlizardite recorded using a 785 nm diode laser.

(Fig. 2). Twinning, probably by reflection on {001}, is observed under crossed polars. The mineral is transparent with a vitreous lustre and has a white streak. It fluoresces greenish-blue when illuminated by a 50 mW 405 nm blue-violet laser (Fig. 1). The Mohs hardness is ~2. Crystals are brittle with irregular fracture and two cleavages: perfect on {001} and good on $\{2\bar{1}0\}$. The mineral is easily soluble in room temperature H_2O. The density could not be measured because the mineral is soluble in Clerici solution and there is insufficient material for physical measurement. The calculated density is 3.469 g cm^{-3} for the empirical formula and 3.507 g cm^{-3} for the ideal formula.

Optically, greenlizardite is biaxial (+), with α = 1.559(1), β = 1.582(1) and γ = 1.608(1), measured in white light. The 2V measured directly on a spindle stage is 88(1)°; the calculated 2V is 87.8°. Dispersion is $r < v$, moderate. The mineral is weakly pleochroic: X = very pale yellow green, Y = pale yellow green and Z = light yellow green; $X < Y < Z$. The optical orientation is $X \approx$ **c**, $Y \approx$ **a** and $Z \approx$ **b***.

Raman spectroscopy

Raman spectroscopy was conducted on a Horiba XploRA PLUS. Pronounced fluorescence was

TABLE 1. Chemical composition (in wt.%) for greenlizardite.

Constituent	Mean	Range	Stand. Dev.	Probe standard	Ideal composition
$(NH_4)_2O$	2.75	1.82–4.02	0.89	Cr_2N (syn.)	2.96
Na_2O	(2.34)	1.80–3.05	0.46	albite	
Na_2O (1 apfu)*	3.34				3.52
UO_3	60.45	58.14–63.60	2.21	UO_2 (syn.)	65.06
SO_3	17.70	16.85–18.87	0.69	celestine	18.21
H_2O**	9.76				10.24
Total*	94.00				99.99

* The low analysis total and lower than expected Na are attributed to the irregular surfaces of mounted crystals. The Na_2O wt.% corresponding to 1 Na apfu is used in the empirical formula.
** Based on the structure.

TABLE 2. Powder X-ray data (d in Å) for greenlizardite. Only calculated lines with $I \geq 2$ are listed.

I_{obs}	d_{obs}	d_{calc}	I_{calc}	hkl
24	13.59	13.6320	25	0 0 1
100	6.80	6.8160	100	0 0 2
12	6.33	6.3486	7	$\bar{1}$ 1 0
36	6.06	6.0695	26	$\bar{1}$ 0 1
62	5.75	5.7730	18	1 $\bar{1}$ 1
		5.7374	25	$\bar{1}$ 1 1
24	5.52	5.5115	18	1 0 1
8	4.65	4.6645	7	1 $\bar{1}$ 2
13	4.53	4.5440	11	0 0 3
		4.4788	2	$\bar{1}$ $\bar{1}$ 1
32	4.41	4.4232	11	0 $\bar{2}$ 1
		4.3904	10	0 2 0
7	4.044	4.0453	4	0 $\bar{2}$ 2
17	3.966	3.9712	7	0 2 1
		3.9399	8	$\bar{1}$ 0 3
13	3.684	3.7093	5	1 $\bar{1}$ 3
		3.6810	9	$\bar{1}$ 1 3
25	3.481	3.4950	18	0 $\bar{2}$ 3
56	3.404	3.4159	10	0 2 2
		3.4109	19	$\bar{2}$ 1 0
		3.4080	14	0 0 4
		3.3589	2	$\bar{2}$ 1 1
4	3.257	3.2610	7	2 $\bar{1}$ 1
6	3.186	3.1863	6	$\bar{1}$ $\bar{2}$ 1
		3.1750	2	$\bar{1}$ 0 4
60	3.126	3.1299	26	$\bar{2}$ 1 2
		3.1166	15	$\bar{1}$ 3 0
26	3.073	3.0772	14	$\bar{1}$ $\bar{2}$ 2
34	2.988	3.0129	4	1 $\bar{1}$ 4
		2.9907	16	1 $\bar{3}$ 2
		2.9764	7	2 $\bar{1}$ 2
18	2.940	2.9531	4	$\bar{1}$ 3 1
		2.9289	9	1 2 1
		2.7345	2	$\bar{2}$ $\bar{1}$ 1
19	2.709	2.7264	6	0 0 5
		2.6998	9	2 1 0
18	2.661	2.6688	5	2 $\bar{3}$ 1
		2.6629	4	$\bar{2}$ $\bar{1}$ 2
		2.6492	4	2 $\bar{1}$ 3
6	2.602	2.6055	4	$\bar{2}$ 3 1
6	2.545	2.5640	4	$\bar{1}$ $\bar{2}$ 4
		2.5345	4	0 $\bar{2}$ 5
11	2.495	2.5072	2	$\bar{2}$ $\bar{1}$ 3
		2.4978	2	$\bar{1}$ 1 5
		2.4903	3	$\bar{2}$ 1 4
		2.4801	3	0 2 4
5	2.456	2.4715	2	1 $\bar{3}$ 4
		2.4226	3	$\bar{1}$ 3 3
7	2.380	2.3808	4	2 1 2
		2.3723	3	1 2 3
		2.2720	3	0 0 6
16	2.254	2.2576	2	$\bar{3}$ 1 1
		2.2537	3	$\bar{3}$ 2 0
		2.2516	2	$\bar{2}$ 3 3
15	2.222	2.2375	2	$\bar{3}$ 2 1
		2.2327	3	0 $\bar{4}$ 1
		2.2222	2	2 $\bar{4}$ 1
		2.1648	2	$\bar{3}$ 2 2
19	2.146	2.1597	3	$\bar{2}$ $\bar{2}$ 3
		2.1539	3	$\bar{2}$ 4 1
		2.1447	3	1 $\bar{1}$ 6
		2.1389	2	$\bar{3}$ 0 1
		2.1367	2	2 2 1
11	2.107	2.1156	3	3 $\bar{2}$ 2
		2.0966	3	$\bar{2}$ $\bar{1}$ 5
		2.0939	2	$\bar{3}$ 1 3
8	2.0796	2.0739	2	2 $\bar{4}$ 3
		2.0673	2	2 $\bar{1}$ 5
		2.0598	2	1 0 6
		2.0508	3	$\bar{3}$ 2 3
13	2.0492	2.0482	2	$\bar{2}$ 3 4
		2.0342	3	$\bar{1}$ $\bar{2}$ 6
7	2.0193	2.0232	2	$\bar{3}$ 0 3
		1.9773	2	2 $\bar{3}$ 5
9	1.9694	1.9661	4	2 1 4
18	1.9400	1.9474	8	0 0 7
		1.9356	4	$\bar{3}$ $\bar{1}$ 1
		1.9275	3	$\bar{1}$ 3 5
26	1.9097	1.9198	2	$\bar{3}$ $\bar{1}$ 2
		1.9156	2	0 $\bar{2}$ 7
		1.9084	4	$\bar{1}$ $\bar{4}$ 2
		1.9047	6	$\bar{3}$ 4 0
		1.8975	2	1 $\bar{5}$ 1
25	1.8817	1.8836	3	1 2 5
		1.8815	3	0 2 6
		1.8784	3	1 4 0
		1.8737	3	$\bar{1}$ 5 0
		1.8683	2	$\bar{3}$ $\bar{1}$ 3
18	1.8553	1.8572	4	3 $\bar{4}$ 2
		1.8557	3	3 1 1
		1.8473	3	3 $\bar{2}$ 4
6	1.8341	1.8386	3	1 $\bar{5}$ 3
10	1.8062	1.8123	3	$\bar{3}$ 4 2
		1.7996	2	$\bar{1}$ $\bar{4}$ 4
12	1.7829	1.7891	2	$\bar{3}$ $\bar{1}$ 4
		1.7838	2	0 $\bar{5}$ 1
		1.7615	2	1 $\bar{3}$ 7
8	1.7283	1.7373	2	$\bar{1}$ 5 2
		1.7269	3	1 4 2
14	1.7016	1.7054	3	$\bar{4}$ 2 0
		1.6930	2	0 $\bar{5}$ 4
13	1.6766	1.6793	4	4 $\bar{2}$ 1
		1.6737	4	1 $\bar{5}$ 5
7	1.6459	1.6491	2	1 $\bar{1}$ 8
		1.6473	3	2 $\bar{1}$ 7
		1.6346	2	$\bar{1}$ $\bar{2}$ 8
		1.6302	2	$\bar{3}$ 4 4
12	1.5912	1.5972	2	3 $\bar{4}$ 5
		1.5955	2	$\bar{4}$ 0 2
		1.5893	2	$\bar{2}$ $\bar{4}$ 1
		1.5879	2	$\bar{3}$ $\bar{1}$ 6
16	1.5671	1.5756	2	$\bar{2}$ $\bar{4}$ 3
		1.5656	2	2 $\bar{6}$ 2
		1.5650	3	$\bar{4}$ 2 4
		1.5599	2	$\bar{1}$ 3 7
		1.5414	2	$\bar{1}$ 5 4
8	1.5213	1.5266	2	1 2 7
		1.5147	3	0 0 9
8	1.5022	1.5025	2	$\bar{3}$ 2 7
7	1.4772	1.4845	2	3 $\bar{6}$ 1
6	1.4546	1.4475	2	3 $\bar{6}$ 3

observed using a 532 nm diode laser; consequently, a 785 nm diode laser was utilized. The spectrum was recorded from 3000 to 50 cm^{-1}; however, only the portion from 1600 to 50 cm^{-1} is shown in Fig. 3 because no features were observed between 3000 and 1600 cm^{-1}.

Quite intense Raman bands at 1225 cm^{-1} and at 1097, 1086 (sh) and 1068 cm^{-1} are attributed to split triply degenerate ν_3 antisymmetric stretching vibrations of the SO_4 tetrahedra. The number of split bands is in line with the presence of two symmetrically non-equivalent SO_4 tetrahedra in the structure of greenlizardite (*cf.* bluelizardite or synthetic klaprothite, Plášil *et al.*, 2016). Bands at 1031 and 1027 (sh) cm^{-1}, having the highest intensity within the region of SO_4 stretching modes, are assigned to the ν_1 symmetric stretching vibrations of SO_4 tetrahedra. A weak, two-component band at 938 and 933 cm^{-1} is assigned to the ν_3 antisymmetric stretching vibration of the uranyl ion, UO_2^{2+}; a very strong band at 837 cm^{-1} is assigned to the ν_1 symmetric U–O stretching vibration of the UO_2^{2+}. The inferred U–O bond lengths (after Bartlett and Cooney, 1989) in the uranyl ion of ~1.77 Å (from ν_1) and 1.76 (from ν_3) are in line with those derived from the present X-ray study.

Weak Raman bands at 635 and 618 cm^{-1} are attributed to the ν_4 (δ) triply degenerated antisymmetric stretching vibrations of SO_4 tetrahedra. Weak Raman bands 469, 450 and 435 (sh) cm^{-1} are related to the split ν_2 (δ) doubly degenerate bending vibrations of the SO_4.

The band at 355 cm^{-1} and possibly also that at 297 cm^{-1} can be attributed to Na–O stretching vibrations (*cf.* Kampf *et al.*, 2015*b*,*c*; Plášil *et al.*, 2010, 2016; Volkovich *et al.*, 1998). The two-component strong Raman band at 234 and 194 cm^{-1}, with shoulders at 258 cm^{-1} and 177 cm^{-1} is most probably related to the ν_2 (δ) doubly degenerate bending vibration of the UO_2^{2+} and U–O_{eq}–*ligand* stretching modes (*cf.* Bullock and Parret, 1970; Ohwada, 1976; Brittain *et al.*, 1985; Plášil *et al.*, 2010). Weak bands at the lowest energies can be assigned to unclassified lattice modes, most probably skeletal vibrations of the whole sheets of polyhedra.

TABLE 3. Data collection and structure refinement details for greenlizardite.

Diffractometer	Rigaku R-Axis Rapid II
X-ray radiation/power	Mo*K*α (λ = 0.71075 Å)/50 kV, 40 mA
Temperature	293(2) K
Structural formula	$(NH_4)Na(UO_2)_2(SO_4)_2(OH)_2 \cdot 4H_2O$
Space group	$P\bar{1}$
Unit-cell dimensions	a = 6.83617(17) Å
	b = 9.5127(3) Å
	c = 13.8979(10) Å
	α = 98.636(7)°
	β = 93.713(7)°
	γ = 110.102(8)°
V	832.49(8) $Å^3$
Z	2
Density (for above formula)	3.492 g cm^{-3}
Absorption coef.	19.794 mm^{-1}
F(000)	776
Crystal size (μm)	100 × 20 × 2
θ range	3.20 to 25.03°
Index ranges	$-6 \le h \le 8$, $-11 \le k \le 11$, $-16 \le l \le 16$
Refl. collected/unique	11,856/2926; R_{int} = 0.037
Refl. with $I > 2\sigma I$	2542
Completeness to θ = 25.03°	99.7%
Refinement method	Full-matrix least-squares on F^2
Parameter/restraints	217/0
Goof	1.070
Final R indices [$I > 2\sigma I$]	R_1 = 0.0239, wR_2 = 0.0491
R indices (all data)	R_1 = 0.0301, wR_2 = 0.0511
Largest diff. peak/hole	+1.24/–0.99 e A^{-3}

$R_{int} = \Sigma|F_o^2 - F_o^2(\text{mean})|/\Sigma[F_o^2]$. Goof = $S = \{\Sigma[w(F_o^2-F_c^2)^2]/(n-p)\}^{1/2}$. $R_1 = \Sigma||F_o|-|F_c||/\Sigma|F_o|$. $wR_2 = \{\Sigma[w(F_o^2-F_c^2)^2]/\Sigma[w(F_o^2)^2]\}^{1/2}$; $w = 1/[\sigma^2(F_o^2)+(aP)^2+bP]$ where a is 0.0151, b is 5.461 and P is $[2F_c^2+\text{Max}(F_o^2,0)]/3$.

Composition

Chemical analyses (6 points on 4 crystals) were performed at the University of Utah on a Cameca SX-50 electron microprobe with four wavelength dispersive spectrometers and using *Probe for EPMA* software. Analytical conditions were 15 kV accelerating voltage, 10 nA beam current and a beam diameter of 5 μm. Counting times were 30 s on peak and 30 s on background for each element. Raw X-ray intensities were corrected for matrix effects with a PAP algorithm (Pouchou and Pichoir, 1991). A time-dependent intensity correction was applied to Na; the N intensity was time independent. Na and N exhibited significant variability, and a negative relationship was apparent. Greenlizardite was very challenging to analyse. It was not possible to obtain a good polish and some

TABLE 4. Atom coordinates and displacement parameters (Å^2) for greenlizardite.

	x/a	y/b	z/c	U_{eq}	U^{11}	U^{22}	U^{33}	U^{23}	U^{13}	U^{12}
NH_4	0.1545(11)	0.3668(7)	0.9677(5)	0.0288(16)	0.041(4)	0.020(4)	0.016(3)	0.001(3)	−0.001(3)	0.002(3)
Na	0.2764(4)	0.0559(3)	0.4990(2)	0.0250(7)	0.0223(16)	0.0296(18)	0.0229(17)	0.0041(14)	0.0003(13)	0.0099(14)
U1	0.13909(4)	0.22166(3)	0.27410(2)	0.01180(8)	0.00982(14)	0.00848(14)	0.01759(15)	0.00406(11)	0.00245(10)	0.00308(11)
U2	0.37132(4)	0.65068(3)	0.27563(2)	0.01173(8)	0.00974(14)	0.00748(14)	0.01776(15)	0.00249(10)	0.00207(10)	0.00268(11)
S1	0.5653(3)	0.06488(19)	0.29872(13)	0.0140(4)	0.0103(8)	0.0100(8)	0.0230(10)	0.0040(7)	0.0043(7)	0.0046(7)
S2	0.9452(3)	0.82295(19)	0.29716(13)	0.0140(4)	0.0081(8)	0.0100(8)	0.0249(10)	0.0055(7)	0.0042(7)	0.0032(7)
O1	0.5528(9)	0.0678(6)	0.4025(4)	0.0297(13)	0.039(3)	0.036(3)	0.020(3)	0.006(3)	0.003(2)	0.019(3)
O2	0.7745(8)	0.1623(6)	0.2812(4)	0.0292(13)	0.015(3)	0.016(3)	0.056(4)	0.008(3)	0.010(3)	0.002(2)
O3	0.4104(7)	0.1195(6)	0.2539(4)	0.0225(12)	0.016(3)	0.018(3)	0.038(3)	0.006(2)	0.003(2)	0.013(2)
O4	0.5235(8)	0.9077(5)	0.2467(4)	0.0199(11)	0.020(3)	0.010(2)	0.031(3)	0.006(2)	0.010(2)	0.004(2)
O5	0.9615(9)	0.8819(6)	0.4013(4)	0.0301(13)	0.031(3)	0.031(3)	0.021(3)	0.002(3)	0.004(2)	0.003(3)
O6	0.7370(7)	0.7066(5)	0.2599(4)	0.0216(12)	0.012(3)	0.011(3)	0.038(3)	0.003(2)	0.003(2)	−0.001(2)
O7	0.1024(8)	0.7516(6)	0.2780(4)	0.0308(14)	0.020(3)	0.018(3)	0.060(4)	0.012(3)	0.007(3)	0.012(2)
O8	0.9814(8)	0.9476(5)	0.2404(4)	0.0204(12)	0.019(3)	0.009(3)	0.032(3)	0.006(2)	0.003(2)	0.003(2)
O9	0.0994(8)	0.2112(6)	0.1458(4)	0.0224(12)	0.029(3)	0.019(3)	0.020(3)	0.006(2)	0.003(2)	0.007(2)
O10	0.1834(8)	0.2309(6)	0.4025(4)	0.0214(12)	0.024(3)	0.016(3)	0.023(3)	0.003(2)	0.001(2)	0.005(2)
O11	0.3130(8)	0.5935(6)	0.1468(4)	0.0217(12)	0.027(3)	0.019(3)	0.019(3)	0.003(2)	0.001(2)	0.008(2)
O12	0.4386(8)	0.7112(6)	0.4043(4)	0.0214(12)	0.022(3)	0.017(3)	0.022(3)	0.002(2)	0.003(2)	0.003(2)
OH1	0.4468(7)	0.4297(5)	0.2810(4)	0.0173(11)	0.012(2)	0.010(2)	0.031(3)	0.006(2)	0.008(2)	0.005(2)
OH2	0.0742(7)	0.4489(5)	0.2970(4)	0.0224(12)	0.011(2)	0.010(3)	0.047(4)	0.008(2)	0.008(2)	0.003(2)
OW1	0.6569(14)	0.8585(10)	0.0431(6)	0.076(3)	0.093(6)	0.085(6)	0.073(6)	0.034(5)	0.029(5)	0.048(5)
OW2	0.7706(11)	0.1127(8)	0.9455(5)	0.0550(19)	0.044(4)	0.063(5)	0.049(4)	0.017(4)	0.000(3)	0.008(4)
OW3	0.3001(12)	0.6217(8)	0.8743(5)	0.0549(19)	0.081(5)	0.059(5)	0.041(4)	0.019(4)	0.017(4)	0.039(4)
OW4	0.7681(10)	0.4831(8)	0.4353(5)	0.0471(17)	0.045(4)	0.067(5)	0.034(4)	0.008(3)	0.002(3)	0.026(4)

beam damage was noted. The low analysis total and lower than expected Na are attributed to the irregular surfaces of mounted crystals. Preliminary analyses on unpolished crystal faces using an Oxford SEMEDX200EDS on a Hitachi S-3000N SEM employing internal standards, while only semi-quantitative, were consistent with stoichiometric Na atom per formula unit (apfu). Because insufficient material is available for a direct determination of H_2O, it has been calculated based upon the structure determination. Analytical data are given in Table 1.

The empirical formula calculated on the basis of 18 O apfu is $(NH_4)_{0.98}Na_{1.00}U_{1.96}S_{2.04}O_{18.00}H_{10.02}$. The ideal formula is $(NH_4)Na(UO_2)_2(SO_4)_2(OH)_2{\cdot}4H_2O$. The Gladstone-Dale compatibility index $1 - (K_P/K_C)$ is –0.016 based on the empirical formula and –0.008 based on the ideal formula, in both cases in the range of superior compatibility (Mandarino, 2007).

X-ray crystallography and structure refinement

The powder X-ray study was carried out using a Rigaku R-Axis Rapid II curved imaging plate microdiffractometer, with monochromatized Mo*K*α radiation (λ = 0.71075 Å). A Gandolfi-like motion on the φ and ω axes was used to randomize the sample. Observed *d* values and intensities were derived by profile fitting using *JADE 2010* software (Materials Data, Inc.). The powder data presented in Table 2 show good agreement with the pattern calculated from the crystal-structure determination.

The single-crystal reflection data were collected using the same diffractometer and with the same radiation as noted above. The *Rigaku CrystalClear* software package was used for processing the data, including the application of both shape-based and empirical absorption corrections, the latter using the multi-scan method with *ABSCOR* (Higashi, 2001). The structure was solved using *SIR2011* (Burla *et al*, 2012). *SHELXL-2013* (Sheldrick, 2015) was used for the refinement of the structure. Difference-Fourier syntheses suggested possible positions for some of the H atoms; however, their reliability was not judged sufficiently high to report. Consequently, they have not been included in the refined structure. The proposed hydrogen-bonding scheme is based upon bond geometries and bond-valence balance, but must be considered highly conjectural. Data collection and refinement details are given in Table 3, atom coordinates and displacement

TABLE 5. Selected bond distances (Å) for greenlizardite.

NH_4–OW3	2.830(9)	Na–O1	2.368(6)	Hydrogen bonds	
NH_4–OW1	2.847(11)	Na–O5	2.371(6)	OH1···OW4	2.824(8)
NH_4–OW2	2.852(9)	Na–O5	2.390(6)	OH2···OW4	2.996(8)
NH_4–O11	2.908(8)	Na–O1	2.418(6)	OW1···OW2	3.039(11)
NH_4–O9	3.049(8)	Na–O10	2.502(6)	OW1···OW3	3.228(12)
NH_4–O6	3.322(9)	Na–O12	2.512(6)	OW2···O8	3.266(9)
<NH_4–O>	2.968	<Na–O>	2.427	OW2···O9	3.26(2)
				OW3···OH1	2.941(9)
U1–O9	1.768(5)	U2–O11	1.768(5)	OW3···OW1	3.228(12)
U1–O10	1.774(5)	U2–O12	1.773(5)	OW4···O10	3.169(9)
U1–OH1	2.325(4)	U2–OH2	2.338(5)	OW4···O12	3.199(8)
U1–OH2	2.333(5)	U2–OH1	2.340(5)		
U1–O2	2.371(5)	U2–O7	2.348(5)		
U1–O3	2.385(5)	U2–O6	2.402(5)		
U1–O8	2.411(5)	U2–O4	2.414(5)		
<U1–O_{Ur}>	1.771	<U2–O_{Ur}>	1.771		
<U1–O_{eq}>	2.365	<U2–O_{eq}>	2.368		
S1–O1	1.447(5)	S2–O5	1.454(6)		
S1–O2	1.472(5)	S2–O7	1.473(6)		
S1–O3	1.472(5)	S2–O6	1.473(5)		
S1–O4	1.481(5)	S2–O8	1.482(5)		
<S1–O>	1.471	<S2–O>	1.468		

parameters in Table 4, selected bond distances in Table 5 and a bond-valence analysis in Table 6.

Description of the crystal structure

The U sites in the structure of greenlizardite are surrounded by seven O atoms forming a squat UO_7 pentagonal bipyramid. This is the most typical coordination for U^{6+}, particularly in uranyl sulfates, where the two short apical bonds of the bipyramid constitute the UO_2 uranyl group. In the structure of greenlizardite, pairs of pentagonal bipyramids share a common edge, forming dimers. The dimers are linked by sharing corners with SO_4 groups, yielding a $[(UO_2)_2(SO_4)_2(OH)_2]^{2-}$ sheet parallel to (001) (Fig. 4). This sheet is based on the phosphuranylite anion topology (Burns, 2005), with a ring symbol $6^1 5^2 4^2 3^2$ (Krivovichev and Burns, 2007). The sheets in johannite, Cu $[(UO_2)_2(OH)_2(SO_4)_2](H_2O)_8$, (Mereiter, 1982), deliensite, $Fe(UO_2)_2(SO_4)_2(OH)_2 \cdot 7H_2O$, (Plášil *et al.*, 2012) and plášilite, $Na(UO_2)(SO_4)(OH) \cdot 2H_2O$ (Kampf *et al.*, 2015*a*) are topologically identical to that in greenlizardite; however, these sheets are geometrical isomers, differing in the orientation of the SO_4 groups (Fig. 4). In greenlizardite, within the same $[(UO_2)_2(SO_4)_2(OH)_2]^{2-}$ sheet, the corner of each SO_4 group that is not shared with UO_7 pentagonal bipyramids points in the same direction.

In the structure of greenlizardite (Fig. 5), the Na bonds to two uranyl O atoms (one in each of two adjacent sheets) and four sulfate O atoms (two in each of two adjacent sheets) yielding an approximately octahedral coordination. NaO_6 octahedra share edges to form zig-zag chains along [100] and these chains link two adjacent $[(UO_2)_2(SO_4)_2(OH)_2]^{2-}$ sheets forming a thick slab. This slab has channels along [100] that

TABLE 6. Bond-valence analysis for greenlizardite. Values are expressed in valence units.*

	NH_4	Na	U1	U2	S1	S2	Hydrogen bonds		Σ
							Accepted	Donated	
O1		0.20			1.60				1.98
		0.18							
O2			0.50		1.50				2.00
O3			0.49		1.50				1.99
O4				0.46	1.47				1.93
O5		0.20				1.57			1.96
		0.19							
O6	0.05			0.47		1.50			2.02
O7				0.53		1.50			2.03
O8			0.46			1.46	+0.09		2.01
O9	0.11		1.80				+0.10		2.01
O10		0.15	1.78				+0.10		2.03
O11	0.16			1.80					1.96
O12		0.14		1.78			+0.10		2.02
OH1			0.55	0.54			+0.14	−0.18	1.05
OH2			0.55	0.54				−0.13	0.96
OW1	0.19						+0.10	−0.12	0.07
								−0.10	
OW2	0.18						+0.12	−0.10	0.11
								−0.09	
OW3	0.20						+0.10	−0.14	0.06
								−0.10	
OW4							+0.18	−0.10	0.11
							+0.13	−0.10	
Σ	0.89	1.06	6.13	6.12	6.07	6.03			

* NH_4^+–O bond valence parameters from Garcia-Rodriguez *et al.* (2000); all other cation–O bond valence parameters from Gagné and Hawthorne (2015); hydrogen-bond strengths based on O–O bond lengths from Ferraris and Ivaldi (1988).

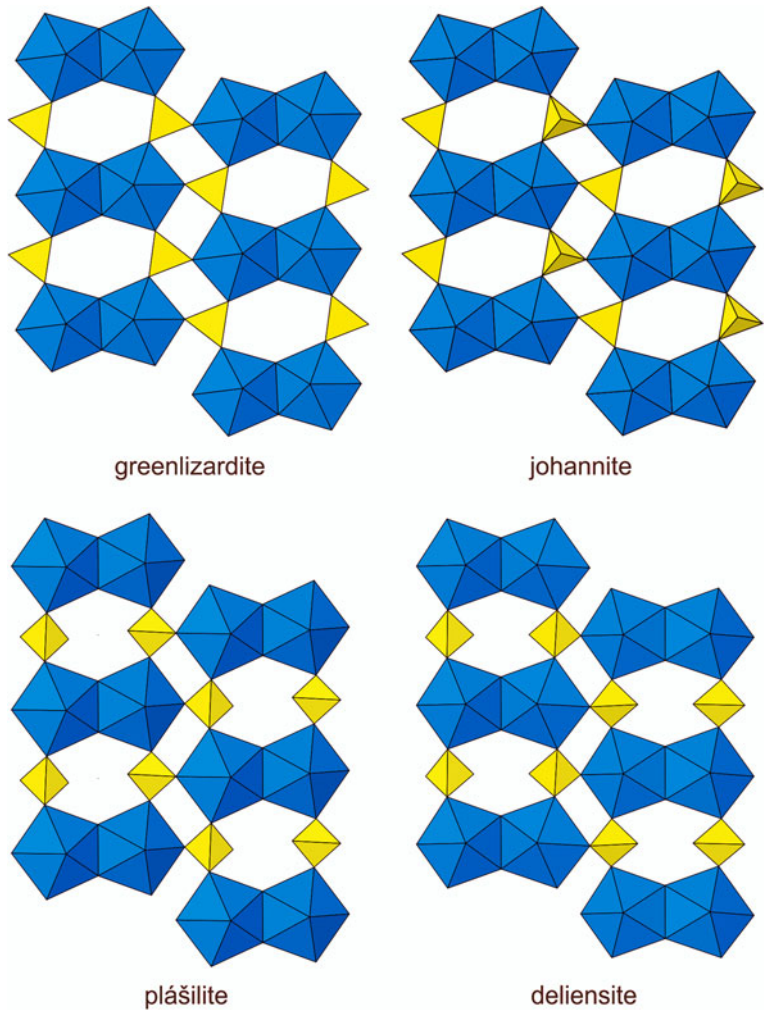

FIG. 4. The uranyl sulfate sheets in greenlizardite, johannite, plášilite and deliensite. UO_7 bipyramids are blue and SO_4 tetrahedra are yellow. Note the differing orientations of SO_4 tetrahedra.

contain isolated H_2O groups (OW4). The NH_4 group and three H_2O groups (OW1, OW2 and OW3) are located in the region between adjacent slabs. The NH_4 bonds to each of the three interlayer H_2O groups (OW1, OW2 and OW3) and links adjacent slabs together by bonding to two uranyl O atoms (O9 and O11) in one slab and one of the equatorial O atoms (O6) of a UO_7 bipyramid in another slab (which is also part of the $S2O_4$ tetrahedron). The NH_4–O6 bond is quite long (3.322 Å), which would be expected to result in very weak linkage between slabs; however, the NH_4–O6 linkage is augmented by extensive hydrogen bonding from the interlayer H_2O groups (OW1, OW2 and OW3).

The linkages between the sheets in the structure of greenlizardite are quite different than those in the structures of johannite, deliensite and plášilite. Most notably, there are two different intersheet regions in greenlizardite, one containing edge-sharing chains of NaO_6 octahedra and the other containing irregular $(NH_4)O_3(H_2O)_3$ polyhedra and they link the sheets together as described above. The structures of johannite, deliensite and plášilite all contain only one type of intersheet region. In deliensite, an individual $Fe^{2+}O(H_2O)_5$ octahedron

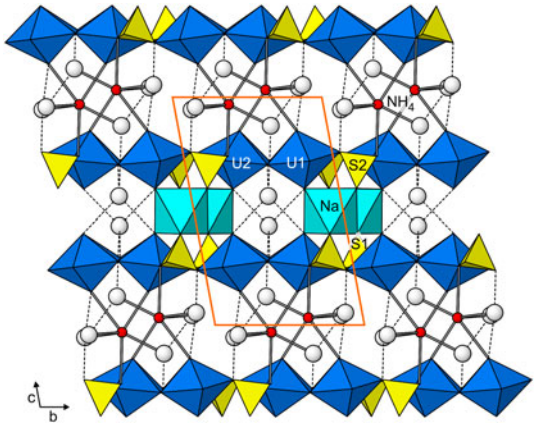

FIG. 5. The structure of greenlizardite viewed down [100]. O atoms of isolated H_2O groups are large white spheres. NH_4–O bonds are shown as sticks. Hydrogen bonds are shown as dashed lines. The unit-cell outline is in orange.

links to one uranyl O atom in one sheet and links to the adjacent sheet only through hydrogen bonding. In johannite, an individual Jahn-Teller distorted $CuO_2(H_2O)_4$ octahedron shares its apical O atoms with uranyl O atoms in two adjacent sheets. In plášilite, $NaO_2(H_2O)_4$ octahedra form a *cis* edge-sharing straight chain and each octahedron shares one O atom with a uranyl group in one sheet and one O atom with a sulfate group in the adjacent sheet.

Acknowledgements

The manuscript benefitted from constructive comments by reviewers Travis Olds and Andrew Locock. This study was funded by the John Jago Trelawney Endowment to the Mineral Sciences Department of the Natural History Museum of Los Angeles County. JP was supported through the project No. 17-09161S of the Grant agency of the Czech Republic.

References

Bartlett, J.R. and Cooney, R.P. (1989) On the determination of uranium-oxygen bond lengths in dioxouranium(VI) compounds by Raman spectroscopy. *Journal of Molecular Structure*, **193**, 295–300.

Brittain, H.G., Ansari, P., Toivonen, J., Niinisto, L., Tsao, L. and Perry, D.L. (1985) Photophysical studies of uranyl complexes. VIII. Luminiscence spectra of $UO_2SO_4 \cdot 3½H_2O$ and two polymorphs of bis(urea) uranyl sulfate. *Journal of Solid State Chemistry*, **59**, 259–264.

Bullock, H. and Parret, F.W. (1970) The low frequency infrared and Raman spectroscopic studies of some uranyl complexes: the deformation frequency of the uranyl ion. *Canadian Journal of Chemistry*, **48**, 3095–3097.

Burla, M.C., Caliandro, R., Camalli, M., Carrozzini, B., Cascarano, G.L., Giacovazzo, C., Mallamo, M., Mazzone, A., Polidori, G. and Spagna, R. (2012) *SIR2011*: a new package for crystal structure determination and refinement. *Journal of Applied Crystallography*, **45**, 357–361.

Burns, P.C. (2005) U^{6+} minerals and inorganic compounds: insights into an expanded structural hierarchy of crystal structures. *Canadian Mineralogist*, **43**, 1839–1894.

Chenoweth, W.L. (1993) *The Geology and Production History of the Uranium Deposits in the White Canyon Mining District, San Juan County, Utah*. Utah Geological Survey Miscellaneous Publication, **93–3**.

Ferraris, G. and Ivaldi, G. (1988) Bond valence vs. bond length in O…O hydrogen bonds. *Acta Crystallographica*, **B44**, 341–344.

Gagné, O.C. and Hawthorne, F.C. (2015) Comprehensive derivation of bond-valence parameters for ion pairs involving oxygen. *Acta Crystallographica*, **B71**, 562–578.

García-Rodríguez, L., Rute-Pérez, Á., Piñero, J.R. and González-Silgo, C. (2000) Bond-valence parameters for ammonium-anion interactions. *Acta Crystallographica*, **B56**, 565–569.

Higashi, T. (2001) *ABSCOR*. Rigaku Corporation, Tokyo.

Kampf, A.R., Kasatkin, A.V., Čejka, J. and Marty, J. (2015*a*) Plášilite, $Na(UO_2)(SO_4)(OH) \cdot 2H_2O$, a new uranyl sulfate mineral from the Blue Lizard mine, San Juan County, Utah, USA. *Journal of Geosciences*, **60**, 1–10.

Kampf, A.R., Plášil, J., Kasatkin, A.V. and Marty, J. (2015*b*) Bobcookite, $NaAl(UO_2)_2(SO_4)_4 \cdot 18H_2O$ and wetherillite, $Na_2Mg(UO_2)_2(SO_4)_4 \cdot 18H_2O$, two new uranyl sulfate minerals from the Blue Lizard mine, San Juan County, Utah, USA. *Mineralogical Magazine*, **79**, 695–714.

Kampf, A.R., Plášil, J., Kasatkin, A.V., Marty, J. and Čejka, J. (2015*c*) Fermiite, $Na_4(UO_2)(SO_4)_3 \cdot 3H_2O$ and oppenheimerite, $Na_2(UO_2)(SO_4)_2 \cdot 3H_2O$, two new uranyl sulfate minerals from the Blue Lizard mine, San Juan County, Utah, USA. *Mineralogical Magazine*, **79**, 1123–1142.

Kampf, A.R., Plášil, J., Kasatkin, A.V., Marty, J., Čejka, J. and Lapčák, L. (2017) Shumwayite, $[(UO_2)(SO_4)(H_2O)_2]_2 \cdot H_2O$, a new uranyl sulfate mineral from Red Canyon, San Juan County, Utah, USA. *Mineralogical Magazine*, **81**, 273–285.

Krivovichev, S.V. and Burns, P.C. (2007) Actinide compounds containing hexavalent cations of the VI group elements (S, Se, Mo, Cr, W). Pp. 95–182 in: *Structural Chemistry of Inorganic Actinide Compounds* (S.V. Krivovichev, P.C. Burns and I.G. Tananaev, editors). Elsevier, Amsterdam.

Mandarino, J.A. (2007) The Gladstone–Dale compatibility of minerals and its use in selecting mineral species for further study. *Canadian Mineralogist*, **45**, 1307–1324.

Mereiter, K. (1982) Die Kristallstrukturs des Johannits, Cu $(UO_2)_2(OH)_2(SO_4)_2 \cdot 8H_2O$. *Tschermaks Mineralogische und Petrographische Mitteilungen*, **30**, 47–57.

Ohwada, K. (1976) Infrared spectroscopic studies of some uranyl nitrate complexes. *Journal of Coordination Chemistry*, **6**, 75–80.

Plášil, J., Buixaderas, E., Čejka, J., Sejkora, J., Jehlička, J. and Novák, M. (2010) Raman spectroscopic study of the uranyl sulphate mineral zippeite: low wavenumber and U–O stretching regions. *Analytical and Bioanalytical Chemistry*, **397**, 2703–2715.

Plášil, J., Hauser, J., Petříček, V., Meisser, N., Mills, S.J., Škoda, R., Fejfarová, K., Čejka, J., Sejkora, J., Hloušek, J., Johannet, J.-M., Machovič, V. and Lapčák, L. (2012) Crystal structure and formula revision of deliensite, $Fe[(UO_2)_2(SO_4)_2(OH)_2](H_2O)_7$. *Mineralogical Magazine*, **76**, 2837–2860.

Plášil, J., Meisser, N. and Čejka, J. (2016) The crystal structure of $Na_6[(UO_2)(SO_4)_4](H_2O)_4$: X-ray and Raman spectroscopy study. *Canadian Mineralogist*, **54**, 5–20.

Pouchou, J.L. and Pichoir, F. (1991) Quantitative analysis of homogeneous or stratified microvolumes applying the model "PAP". Pp. 31–75 in: *Electron Probe Quantification*, (K.F.J. Heinrich and D.E. Newbury, editors). Plenum Press, New York.

Sheldrick, G.M. (2015) Crystal structure refinement with SHELXL. *Acta Crystallographica*, **C71**, 3–8.

Volkovich, V.A., Griffiths, T.R., Fray, D.J. and Fields, M. (1998) Vibrational spectra of alkali metal (Li, Na and K) uranates and consequent assignment of uranate ion site symmetry. *Vibrational Spectroscopy*, **17**, 83–91.